20. GLOBAL COSMOLOGICAL PARAMETERS: H_0, Ω_M, and Λ

Written April 2000 by M. Fukugita (University of Tokyo, Institute for Cosmic Ray Research) and C.J. Hogan (University of Washington).

This review surveys the current status of the determination of the three cosmological parameters, the Hubble constant H_0, the mass density parameter Ω_M and the cosmological constant Λ. These quantities set the scale and characterize the mean mass-energy content and curvature in cosmological solutions of Einstein's equations which describe the geometry and evolution of the universe as a whole. For technical details, see Ref. 1.

We adopt the normalization $\Omega_M + \Omega_\Lambda = 1$ for zero curvature (flat universe), where $\Omega_\Lambda = \Lambda/3H_0^2$ with Λ being the cosmological constant entering in the Einstein equation. The case with $\Omega_M = 1$ and $\Omega_\Lambda = 0$ is referred to as the Einstein-de Sitter (EdS) universe. We often use distance modulus $m - M = 5\log(d_L/10 \text{ pc})$ instead of the luminosity distance d_L, where m is the apparent magnitude of an object whose magnitude at 10 pc would be M. We omit the unit km s^{-1}Mpc^{-1} for the Hubble constant and adopt the abbreviation $h = H_0/100$.

20.1. The Hubble Constant

20.1.1. ***Overview***: The Hubble constant, which has dimension of inverse time, sets the scale of the size and age of the Universe. Recent efforts to measure it have almost solved the long-standing discrepancy concerning the extragalactic distance scale; at the same time, new uncertainties have been revealed in the Milky Way distance scale.

The global value of H_0 was uncertain by a factor of two for several decades. Before 1980 the dispute was between two schools: Sandage and collaborators insisted on $H_0 = 50$; de Vaucouleurs and collaborators preferred a high value, $H_0 = 90$–100. The dichotomy persisted even after the discovery of an empirical but tight relationship between a galaxy's luminosity and rotation velocity, known as the Tully-Fisher relation, which allowed relative distances between whole galaxies to be estimated far out into the smooth Hubble flow. A straightforward reading of the Tully-Fisher relation gave values $H_0 = 80$–90, but this result was challenged over the issue of the Malmquist bias—whether the sample selects preferentially bright galaxies, biasing towards a shorter distance. A related dispute concerned the distance to the Virgo cluster, 16 Mpc or 22 Mpc, depending on the sample used.

The next major advance came in 1989–1990 when new, more precise relative distance indicators were discovered: the apparently universal shape of the the planetary nebula luminosity function (PNLF), and the surface brightness fluctuations (SBF) in galaxy images, utilizing the fact that a more distant galaxy shows a smoother light distribution. The two completely independent methods predicted relative distances to individual galaxies in excellent agreement with each other, and also with the Tully-Fisher relation (albeit with a somewhat larger scatter) [2]. These new techniques, when calibrated with the distance to M31, yielded a value around $H_0 = 80$ and a Virgo distance of 15 Mpc.

Around the same time Type Ia supernovae (SNeIa) were widely adopted as standard candles. This led to $H_0 = 50$–55, when calibrated with a Cepheid distance to the nearest SNIa host galaxy using the pre-refurbished *Hubble Space Telescope* (HST). Thus in the early nineties estimates were still dichotomous between $H_0 = 50$ and 80.

The refurbishment of HST allowed accurate measurements of Cepheids in galaxies as distant as 20 Mpc. This secured the distance to the Virgo cluster and tightened the calibrations of the extragalactic distance indicators, and resulted in $H_0 = (70$–$75) \pm 10$, 10% lower than the 'high value'. Another important contribution was the discovery that the maximum brightness of SNeIa varies from supernova to supernova, and that it correlates tightly with the decline rate of brightness. Direct calibration of the maximum brightness of several SNeIa with HST Cepheid observations yielded $H_0 = 65^{+5}_{-10}$, and nearly resolved the long-standing controversy.

All the methods mentioned above use distance ladders and take the distance to the Large Magellanic Cloud (LMC) to be 50 kpc ($m - M = 18.5$) as the zero point. Before 1997 few doubts were cast on the distance to LMC. With the exception of determinations using RR Lyr stars, the distance modulus converged to $m - M = 18.5 \pm 0.1$, *i.e.*, with a 5% error, and the RR Lyr discrepancy was blamed on its larger calibration error. It had been believed that the Hipparcos astrometric satellite would secure the distance within the Milky Way and tighten the distance to LMC. To everyone's surprise, Hipparcos instead revealed the contrary: the distance to LMC was more uncertain than we had thought, introducing new uncertainties into the determination of H_0. Connected to this, the age of the Universe turned out to be more uncertain than had been believed.

20.1.2. ***Extragalactic distance scale***: The measurement of cosmological distances traditionally employs distance ladders, as shown in Table 20.1. The listings written in italics indicate new methods which circumvent intermediate rungs. The most important milestone of the ladder is the LMC distance, 50 kpc ($m - M = 18.5$). The century-old Cepheid period-luminosity (PL) relation is still given great weight, but requires a few lower rungs to calibrate its zero point.

The refurbishment of the HST achieved sufficient resolution to resolve Cepheids in the Virgo cluster [3]. Now 28 nearby spiral galaxies within 25 Mpc are given distances measured using the Cepheid PL relation [4]. A typical random error is 4–5% (0.08–0.10 mag), and the systematic error (from photometry) is 5% (0.1 mag) excluding the uncertainty of the LMC distance, to which the HST-KP ("Key Project") group assigns 6.5% error (0.13 mag). The prime use of these galaxies is to calibrate secondary distance indicators, which penetrate to sufficient depth that perturbations in the Hubble flow are a minor component of the error budget. The results, summarized in Table 20.2, include a few earlier SNIa results which employed a partial list of Cepheid calibrators.

We emphasize H_0 determinations by two methods, SBF and SNeIa, in particular those underlined in the table. A cross correlation analysis showed that the relative distances agree well between SBF and others, including the Cepheids [5,6], and that it is probably the best secondary indicator presently available together with SNeIa. It is also important that there are now 300 galaxies measured with SBF, which are essential to make corrections for peculiar velocity flows for the ≤ 4000 km s^{-1} sample. The final

Table 20.1: Traditional distance ladders.

Method	Distance range	typical targets
Population I stars		
trigonometric or kinematic methods (ground)	< 50 pc	Hyades, nearby dwarfs
main sequence fitting (FG stars) Pop. I	< 200 pc	Pleiades
trigonometric method (Hipparcos)	< 500 pc	nearby open clusters
main sequence fitting (B stars)	40 pc–10 kpc	open clusters
Cepheids [Population I] (ground)	1 kpc–3 Mpc	LMC, M31, M81
Cepheids [Population I] (HST)	< 30 Mpc	Virgo included
secondary (extragalactic) indicators	700 kpc–100 Mpc	
Population II stars		
trigonometric method (Hipparcos)	< 500 pc	nearby subdwarfs
subdwarf main sequence fitting	100 pc–10 kpc	global clusters
cluster RR Lyr	5 kpc–100 kpc	LMC, age determinations

Table 20.2: Hubble constant (uncertainties in the LMC distance are not included).

Secondary indicators	References	Hubble constant
Tully-Fisher	HST-KP (Sakai *et al.*, [8])	$71 \pm 4 \pm 7$
Fundamental plane	HST-KP (Kelson *et al.*, [9])	$78 \pm 8 \pm 10$
SBF	HST-KP (Ferrarese *et al.*, [10])	$69 \pm 4 \pm 6$
SBF	Tonry *et al.*, [7]	$\underline{77 \pm 4 \pm 7}$
SBF (galaxy z survey)	Blakeslee *et al.*, [11]	$74 \pm 4 \pm 7$
SNeIa	Riess *et al.*, [12]	67 ± 7
SNeIa	Hamuy *et al.*, [13]	$63 \pm 3 \pm 3$
SNeIa	Jha *et al.*, [14]	$64.4^{+5.6}_{-5.1}$
SNeIa	Suntzeff *et al.*, [15]	65.6 ± 1.8
SNeIa	HST-KP (Gibson *et al.*, [16])	$\underline{68 \pm 2 \pm 5}$
SNeIa	Saha *et al.*, ([17])	60 ± 2

value of Tonry *et al.* [7] is $H_0 = 77 \pm 8$, in which ± 4 is allotted to uncertainties in the flow model and another ± 4 to SBF calibration procedure in addition to the error of the Cepheid distance ± 6 (a quadrature sum is taken). When supplemented with peculiar velocity information from redshift surveys of galaxies, the value is further constrained to be 74 ± 4 up to the Cepheid distance error [11].

It is impressive that analyses of SNeIa Hubble diagram give virtually the same answer despite differences and corrections. The smaller H_0 of Saha *et al.* [17] arises from omission of the luminosity-decline rate correction; including this would push H_0 up by 10%. The other notable difference is a slightly higher value of HST-KP. Gibson *et al.* [16] made a reanalysis for all Cepheid observations performed by other groups and showed that the distances are all farther than would be derived from the HST-KP procedure. Taking the luminosity-decline rate correlation to be real and adopting Cepheid distances from the HST-KP data reduction, we adopt $H_0 = 68$ from SNeIa.

Leaving out the uncertainty of the Cepheid distance, H_0 from Tonry *et al.*'s [7] SBF determination is 77±6, and that from SNeIa (HST-KP) is 68±4. The difference is 13%, and the two values overlap at $H_0 = 71$. Allowing for individual 2σ errors, the overlap is in a range of $H_0 = 65$–76. An additional uncertainty is the 6% error ($\delta H_0 = \pm 4.5$) from the Cepheid distance which is common to both, still excluding the uncertainty of the LMC distance. We may summarize $H_0 = 71 \pm 7$ or 64–78 as our current standard, provided that the LMC distance is 50 kpc.

The convergence is a great achievement, in spite of the fact that the SNeIa results are still lower than those from other secondary indicators by 10%. All analyses are based on the LMC distance modulus $m - M = 18.50$ [18,19]. Doubts about this distance are discussed next.

20.1.3. ***The Local Distance Scale: Distance to LMC***: Most traditional paths to the LMC distance follow the ladder shown in the upper half of Table 20.1. The Hipparcos satellite can measure a parallax as small as 2 milliarcsec (mas), corresponding to a distance of 500 pc. It was a reasonable expectation that the geometric distance to the Pleiades cluster could be determined, circumventing the main sequence fitting from nearby parallax stars to the Pleiades and thus securing the Galactic distance scale. Hipparcos results have also opened new methods to estimate the distance to the LMC. However, the new detailed information has actually brought confusion.

The "Pleiades problem": The Pleiades cluster at 130 pc has long been taken to be the first milestone of the distance work, since it has nearly solar abundance of heavy elements. Hipparcos results have led to a revision of the previous distance modulus, based on main sequence fitting of FGK dwarfs, shorter by 0.25 mag (12%) [20,21]. This is a serious problem, since the disagreement means that either our understanding of FGK dwarfs, for which we have the best knowledge about stellar evolution, is incomplete, or that the Hipparcos parallax measurements contain systematic errors [22,23].

Metallicity effects in the LMC Cepheid calibration: The Cepheid distance to LMC is based on calibration using open cluster Cepheids, the distances to which are estimated by B star main sequence fitting that ties to the Pleiades (see Ref. 18 and references therein). It is shown that the residual of the PL fit shows a strong metallicity (Z) dependence. This means *either* the Cepheid PL relation suffers from a large Z effect, or the distances to open clusters contain significant Z-dependent errors [24]. A correction for this effect changes the distance to LMC either way, depending upon which interpretation is correct. So far direct Hipparcos Cepheid distances are too noisy to resolve this issue directly [25–27].

Red clump: Hipparcos has recalibrated the "red clump," the He burning stage of Population I stars, giving the distance modulus to LMC as 18.1±0.1. Although much shorter than distances from other methods, this value is substantially in agreement with earlier red clump results [28,29].

Eclipsing binaries: Double-spectroscopic eclipsing binaries in principle yield the distance in a semi-geometric way out to LMC or even farther. The LMC distance modulus is estimated to be $m - M = 18.30 \pm 0.07$ [30]. There is a claim that the extinction used is too small by an amount of $\Delta E(B-V) = 0.037$ mag, leading to $m - M = 18.19$ [31].

RR Lyr calibration: The absolute luminosity of RR Lyr depends on metallicity, usually expressed as

$$\langle M_V(\text{RR Lyr})\rangle = a[\text{Fe/H}] + b \ . \tag{20.1}$$

(V means values obtained using a "visual" wideband filter.) Considerable effort has been invested in determining the coefficients (a, b). The problem is again how to estimate the distance to RR Lyr stars. The calibration from the ground, $(a, b) = (0.2, 1.04)$, leads to an LMC distance of $m - M \approx 18.3$. Using Hipparcos field subdwarfs with parallax to calibrate RR Lyr in globular clusters gives $(a, b) = (0.22 \pm 0.09, 0.76)$, which brings the LMC distance to $m - M = 18.5$–18.6 [32]; see also Ref. 33. Statistical parallax for field RR Lyr in the Hipparcos catalogue [34,35], however, agrees better with the ground-based estimate. The uncertainties of 0.3 mag in the RR Lyr calibration translate to the LMC distance modulus 18.25–18.55.

Summary of the LMC distance problem: The distance modulus of the LMC is now uncertain by as much as 0.4 mag (20% in distance), ranging from 18.20 to 18.60. Recent observations with new techniques argue for the lower value. There is clearly a systematic effect, so that we cannot simply take an 'average of all observations'. Rather, we should leave both possibilities open.

20.1.4. ***Direct and Physical Methods***: Techniques called 'physical methods,' allow distance estimates without resorting to astronomical ladders. The advantage of the ladder is that the error of each ladder can be well documented, while the disadvantage is accumulation of errors. Physical methods are free from 'accumulation of errors,' but in this case the central problem is to minimize the model dependence and document realistic systematic errors. (The use of SNeIa maximum brightness was once taken to be a physical method; when it was 'downgraded' to an empirically-calibrated ladder, the accuracy and reliability were significantly enhanced.) A few direct results are reliable enough to be compared with the distances from ladders.

Geometrical calibration of the Cepheids: NGC4258 (M106) shows H_2O maser emission from clouds orbiting around a black hole of mass $4 \times 10^7 M_\odot$ located at the center. Precise VLBA measurements of Doppler velocities show that the motion of the clouds is very close to Keplerian and is perturbed very little. A complete determination is made for the orbital parameters, including centripetal acceleration and a bulk proper

motion of the emission system. This yields a geometric distance to NGC4258 to be 7.2 ± 0.3 Mpc [36]. The distance is also measured using the conventional Cepheid PL relation to give 8.1±0.4 Mpc with $(m - M)_{\rm LMC} = 18.5$, 13% longer than that from the maser measurement [37]. The short LMC distance would bring the Cepheid distance in a perfect agreement with the geometric distance. However, this is only one example, and the difference could be merely a statistical effect: the deviation is only twice the error.

Expansion photosphere model (EPM) for Type II supernovae (SNeII): If a supernova is a black body emitter one can calculate source brightness from temperature. The distance can then be estimated by comparing source brightness with the observed flux. In SNeII atmospheres the flux is diluted due to electron scattering opacity, requiring more sophisticated model atmospheres. Schmidt *et al.* [38,39] developed this approach and obtained absolute distances of SNeII in agreement with those from the ladder. The Hubble constant they obtained is 73±9.

Gravitational lensing time delay: When a quasar image is split into two or more by gravitational lensing, a time delay arises among images from different path lengths and potentials at the image postition of the galaxy. The time delay is written as a product of a cosmological factor and a deflector model. It is observable if the source is variable, and can be used to infer H_0 [40]. The cosmological factor depends on Ω_M only weakly; its Ω_Λ dependence is even weaker. However, a crucial ingredient in this argument is a well-constrained model of the mass distribution of the deflector.

The first estimates of H_0 used the 0957+561 lens system. The deflector is not simple but includes a giant elliptical galaxy embedded in a cluster. There is an ambiguity associated with a galaxy mass/cluster mass separation, which does not change any observed lens properties but affects the derived Hubble constant. One way to resolve this degeneracy is to use the velocity dispersion of the central galaxy [41]. While the long-standing issue as to the value of the time delay was settled and $H_0 = 64 \pm 13$ was reported [42], the inclusion of a wider class of models [43] produces a significantly wider range, $H_0 = 77^{+29}_{-24}$, representing uncertainties associated with the choice of models. The second example, PG1115+080, is again not a simple deflector but includes an elliptical galaxy embedded in a compact group of galaxies. Various models for this system yield $H_0 = 36$–70 [44–47], but, as is discussed in the papers, the derived H_0 depends on the assumption for the dark matter distribution, with H_0 varying from 44±4 to 65 ± 5.

Recently time delays have been measured for three simpler lenses, B0218+357, B1608+656 and PKS1830-211. Among them B0218+357 is a rather clean, isolated spiral galaxy lens, giving $H_0 = 69^{+13}_{-19}$ (the central value will be 74 if $\Omega_M = 0.3$) with a simple galaxy model of a singular isothermal ellipsoid [48]. For B1608+656 one obtained 64±7 for $\Omega_M = 0.3$ (59±7 for an EdS universe) and for PKS1830-211 75^{+18}_{-10} for EdS and 85^{+20}_{-11} for $\Omega_M = 0.3$ from the time delay measured by Koopmans and Fassnacht [49]. These authors concluded 74 ± 8 for low density cosmologies (69 ± 7 for EdS) from four (excluding the second) lensing systems with the simplest model of deflectors. It is encouraging to find such good agreement with the values from ladders from completely independent arguments.

Zeldovich-Sunyaev effect: The observation of the Zeldovich-Sunyaev (ZS) effect (the statistical heating of background photons by Compton scattering off hot electrons) for clusters tells us about the cluster depth (times electron density), which, when combined with angular diameter (times electron density squared) from x-ray observations, gives us the distance to the cluster provided that the cluster is spherical [50–52]. Although new and promising samples of ZS data are being assembled [52], we give little weight to this method for the time being since it is still subject to large systematic errors (±30%). Even with a large sample, selection effects would bias towards clusters elongated along the line of sight because of higher surface brightness.

20.1.5. ***Age of globular clusters***: The most restrictive estimate for cosmic age is obtained from the evolution of globular clusters. Here, the RR Lyr calibration is also crucial, since the stellar age is proportional to the inverse of luminosity, *i.e.*, inverse square of the distance. Modern calculated evolutionary tracks of the main sequence by different authors agree reasonably well. There are occasional disagreements of colors at around the turn-off point, largely depending on the treatment of convection, but the turnoff luminosity is little affected (see *e.g.*, Renzini [53] and VandenBerg *et al.* [54]). The absolute magnitude at the turn-off point M_V^{TO} of the main sequence is hence a good indicator of the age [53]:

$$\log t_9 = -0.41 + 0.37 M_V^{TO} - 0.43\, Y - 0.13[\mathrm{Fe/H}]\ , \tag{20.2}$$

in units of Gyr, or

$$\log t_9 = -0.41 + (0.37a - 0.13)[\mathrm{Fe/H}] + 0.37[(M_V^{TO} - M_V^{\mathrm{RR}}) + b] - 0.43\, Y \tag{20.3}$$

if Eq. (20.1) is inserted. (Y is the helium mass fraction.) The difference of the magnitudes between the turn-off point and RR Lyr ($M_V^{TO} - M_V^{\mathrm{RR}}$) depends little on clusters and is measured to be 3.5±0.1 mag [55]. The a dependence appears in such a way that the metallicity dependence of the cluster age disappears if $a = 0.35$, *i.e.*, globular cluster formation appears coeval [56]. Current estimates (see above) give $a \approx 0.2$, which indicates that metal-poor clusters appear older.

The dichotomous calibrations of RR Lyr stars obviously affect the age of globular clusters. The result also depends on whether one takes the age-metallicity correlation to be real, as indicating metal-poor clusters being formed earlier, or merely due to a systematic error, the formation of globular clusters being coeval. The possibilities are four-fold:

b	$(m-M)_{\mathrm{LMC}}$	t_0 (noncoeval)	t_0 (coeval)
1.05	18.25	18 Gyr	15 Gyr
0.75	18.55	14 Gyr	12 Gyr

In addition there are ±10% errors of various origin. The recent claims of Gratton *et al.* [32], Reid [33], and Chaboyer *et al.* [57] for young universe (11–12 Gyr) assume a coeval-formation interpretation together with the long RR Lyr calibration and the mean of globular cluster ages. The three other possibilities, however, are not excluded.

20.1.6. ***Conclusions on H_0***: Progress in the extragalactic distance scale has been substantial. The ladders yield values convergent within 10%, compared to a factor of 1.6 disagreement in early nineties. A new uncertainty, however, becomes manifest in the Galactic distance scale: there is a 15–20% uncertainty in the distance to LMC. Therefore, we may summarize

$$H_0 = (71 \pm 7) \times^{1.15}_{0.95} \tag{20.4}$$

as a currently acceptable value of the Hubble constant. This agrees with a HST-KP summary of Mould *et al.* [58] up to the uncertainty from the LMC distance, though we followed a different argument. This still allows $H_0 = 90$ at the high end (if Tonry *et al.*'s SBF [7,11] is given a higher weight) and 60 at the low end (if the SNeIa results are weighted). Note that H_0 from both EPM and gravitational lensing are consistent with the ladder value for $(m - M)_{\rm LMC} = 18.5$. With the shorter LMC distance the overlap is marginal.

The short LMC distance also causes trouble for H_0-age consistency. The LMC distance modulus of $m - M = 18.25$ would raise the lower limit of H_0 to 72, and increase the lower limit of age from ≈11.5 Gyr to ≈14.5 Gyr at the same time. There is then no solution for a $\Lambda = 0$ universe. Even with a non-zero Ω_Λ the solution is marginal (see Fig. 20.1 below).

20.2. The Density Parameter

The dimensionless cosmological density parameter directly controls the gravitational formation of cosmic structure. As our understanding of the cosmic structure formation is tightened, we should have a convergence of the Ω_M parameter. An important test is to examine whether estimates of Ω_M parameter extracted from cosmic structure formation agree with each other and with the values estimated in more direct ways.

20.2.1. ***Model-independent determinations***:

Luminosity density × $\langle M/L \rangle$: The mass density can be obtained by multiplying the luminosity density ($\mathcal{L}_B = (2.0 \pm 0.4) \times 10^8 h L_\odot$ Mpc^{-3}) with the average mass-to-light ratio $\langle M/L \rangle$. The M/L_B of galaxies is about 1–2 in galaxy disks and generally increases with the scale due to the increasing dominance of dark matter. If the dark matter distribution is isothermal within the virial radius ($r = 0.13$ Mpc $\Omega_M^{-0.15} [M/10^{12} M_\odot]^{1/2}_{<100\ \rm kpc}$ in a spherical collapse model), the value of M/L_B inside the virial radius is (150–400) h for L^* galaxies. This is about the value of M/L_B estimated for groups and clusters, (150–500)h, both from dynamics [59] and from lensing, (see *e.g.*, Kaiser *et al.* [60]). Multiplying the two values we get [61] $\Omega_M = 0.20 \times 2^{\pm 1}$. The CNOC group [62] made a self-contained estimate using their cluster sample and built-in field galaxy sample. They estimated $M/L_r \approx (210 \pm 60)\, h$ (n.b.: $M/L_B \approx 1.4 \times M/L_r$) for field galaxies from the cluster value $(289 \pm 50)h$. Their luminosity density of field galaxies is $\mathcal{L}_r = (1.7 \pm 0.2) \times 10^8 h L_\odot$ Mpc^{-3}, and therefore $\Omega_M = 0.19 \pm 0.06$.

H_0 versus cosmic age: For $H_0 \geq 60$, the age is 10.9 Gyr for the EdS universe. Since this is too short, Ω_M must be smaller than unity. The limits on H_0 and Ω_M are best compared graphically (see Fig. 20.1 below).

Type Ia supernova Hubble diagram: The type Ia supernova Hubble diagram now reaches $z \approx 0.4$–0.8. It can be used to infer the mass density parameter and the cosmological constant. As we discuss later, the observations favor a low Ω_M and a positive Λ. If we accept the published formal errors, $\Omega_M > 0.1$ is allowed only at three sigma for a zero Λ universe [63,64]. With some allowance for systematic effects, a zero Λ open universe may not be excluded yet, but an EdS geometry is far away from the observations. The favored value for Ω_M is approximately $0.8\ \Omega_\Lambda - 0.4$.

Baryon fractions in Galaxy Clusters: If the gas in a galaxy cluster is in approximate hydrostatic equilibrium (at the virial temperature $T \approx 7 \times 10^7 (\sigma/1000\ \mathrm{km\ s^{-1}})^2$ K), its mass can be estimated by the luminosity and temperature of x-ray emission. In typical clusters baryon mass in the gas exceeds that in stars by an order of magnitude, so the gas gives the total baryon mass [65,66]. From 19 clusters White and Fabian [67] obtained $M_{\rm gas}/M_{\rm grav} = 0.056\ h^{-2/3}$, where $M_{\rm grav}$ is the dynamical mass. By requiring that the cluster baryon fraction agrees with Ω_B/Ω_M in the field, we have $\Omega_M = 0.066\ h^{-1/2}\eta_{10} = 0.39\ (\eta_{10}/5)$, where η_{10} is the global baryon to photon ratio in units of 10^{-10} and the last number assumes $h = 0.7$. An independent estimate from the Zeldovich-Sunyaev effect observed in clusters [51,68] yields $M_{\rm gas}/M_{\rm grav} = 0.082\ h^{-1}$, or $\Omega_M = 0.044\ h^{-1}\eta_{10} = 0.31\ (\eta_{10}/5)$. With $\eta_{10} = 3$–5 from primordial nucleosynthesis (see Sec. 19 on "Big-bang nucleosynthesis" in this *Review*) we have $\Omega_M = 0.2$–0.4.

Nonlinear Statistical Dynamics on Small Scales: For small scales ($r < 1$ Mpc) perturbations are non-linear, and a statistical equilibrium argument is invoked for ensemble averages: the peculiar acceleration induced by a pair of galaxies is balanced by relative motions (the cosmic virial theorem). Current estimates [69] give $\Omega_M(10\ \mathrm{kpc} \lesssim r \lesssim 1\ \mathrm{Mpc}) = 0.15 \pm 0.10$ from the pairwise velocity dispersion (with samples excluding clusters) and the three point correlation function of galaxies via a statistical stability argument. Least action principle reconstruction of galaxy orbits in the Local Group gives $\Omega_M = 0.15 \pm 0.15$. All arguments involving velocity are uncertain regarding the extent to which galaxies trace the mass distribution (biasing), or how much mass is present far away from galaxies.

Simple quasi-linear infall models: For larger scales ($r > 10$ Mpc), where perturbations are still in a linear regime, the velocity field is described by

$$\nabla \cdot \vec{v} + H_0\, \Omega_M^{0.6}\, \delta = 0\ , \tag{20.5}$$

where δ is the enclosed mass overdensity. An integral form of Eq. (20.5) for a spherically symmetric case, $v/H_0 r = \Omega_M^{0.6}\langle\delta\rangle/3$, when applied to the Virgocentric flow, gives $\Omega_M \approx 0.2$ for $v \approx 200$–400 km s^{-1} and $\langle\delta\rangle \sim 2$, assuming no biasing, *i.e.*, galaxies mass [70]. Recently, Tonry *et al.* [7] argued that the peculiar velocity ascribed to the

Virgo cluster is only $\lesssim$140 km s^{-1}, while the rest of the peculiar velocity flow is attributed to the Hydra-Centarus supercluster and the quadrupole field.

Large-scale velocity flows: There are several methods to statistically compare large-scale velocity flows and density perturbations [71,72]. If δ is measured from galaxy clustering, Ω_M always appears in the measured combination $\beta = \Omega_M^{0.6}/b$ where b is a linear biasing factor of galaxies against the mass distribution. The value of $\Omega_M^{0.6}/b$ varies from 0.3 to 1.1, and tends to favor a high value. The most recent POTENT analysis using the Mark III compilation of velocities indicates a high-density universe, $\Omega_M = 0.5$–0.7 with $\Omega_M < 0.3$ excluded at a 99% CL [73]. Blakeslee *et al.* [11] derived $\Omega_M \approx 0.25 \pm 0.05$, if b is close to unity, using better-determined distances from SBF. In spite of substantial effort the results are controversial. The difficulty is that one needs accurate information for velocity fields, for which an accurate estimate of distances *and their errors* is crucial. Random errors of the distance indicators introduce large noise in the velocity field. This seems particularly serious in the POTENT algorithm, in which the derivative $\nabla \cdot \vec{v}/\Omega_M^{0.6}$ and its square are numerically computed. This procedure enhances noise, especially for a small Ω_M.

20.2.2. ***Model-dependent determinations***: The following derivations of the mass density parameter are based on the hierarchical clustering model of cosmic structure formation assuming the cold dark matter (CDM) model. The extraction of Ω_M is therefore indirect. On the other hand it is reasonable to appeal to such models, since Ω_M is the parameter that predominantly controls gravitational structure formation.

Shape parameter of the transfer function: Perturbations of density are described by the Fourier power spectrum $P(k)$, where k is the spatial wavenumber. CDM models predict a shape for the linear power spectrum $P(k) \propto k^{n-4}$ on small scales and $P(k) \propto k^n$ on large scales, where $n \approx 1$ is the primordial power law index. The transition scale is determined by $k_{eq} \approx 2\pi/c\,t_{eq}$, where the characteristic length $c\,t_{eq} = 6.5(\Omega_M h)^{-1}h^{-1}$ Mpc is the horizon size at the time of matter-radiation equality (in comoving units, appropriately stretched to the present epoch). The "shape parameter" $\Gamma \equiv \Omega_M h$ can be estimated from galaxy clustering, and to yield sufficient clustering power on scales of tens of Mpc must be small, about 0.2 [74–76].

Power spectrum in nonlinear galaxy clustering: It is argued that the power spectrum in a small scale region ($k^{-1} < 3h^{-1}$ Mpc), where nonlinear effects are dominant, shows more power than is expected in $\Omega_M = 1$ cosmological models. The excess power is understood if $\Omega_M \approx 0.3$ [77].

Evolution of the rich cluster abundance: The cluster abundance at $z \approx 0$ requires the rms mass fluctuation $\sigma_8 = \langle(\delta M/M)\rangle^{1/2}|_{r=8h^{-1}\ \mathrm{Mpc}}$ to satisfy $\sigma_8 \approx 0.6\ \Omega_M^{-0.5}$ [78,79]. The evolution of the cluster abundance is sensitive to σ_8 in early epochs of growth, corresponding to $z \gtrsim 0.3$ for rich clusters. The rich cluster abundance at $z \sim 0.3$–1, when compared with that at a low z, thus determines both σ_8 and Ω_M [80]. Carlberg [81] derived $\Omega_M = 0.4 \pm 0.2$, and Bahcall and Fan [82] obtained $\Omega_M = 0.2^{+0.3}_{-0.1}$, while Eke *et al.* [76] reported $\Omega_M = 0.43 \pm 0.25$ for an open universe, and $\Omega_M = 0.36 \pm 0.25$ for

a flat universe, corresponding to a slow growth of the abundance. On the other hand, Blanchard and Bartlett [83] and Reichart *et al.* [84] obtained $\Omega_M \approx 1$ from a more rapid growth. The controversy among authors arises from different estimates of the cluster mass at high z.

Cluster abundance versus the COBE normalization: The cluster abundance gives an accurate estimate of σ_8 for a low-z universe. Another place we can extract an accurate σ_8 is from the fluctuation power imprinted on cosmic microwave background radiation (CBR) anisotropies. Assuming the model CDM transfer function $\sigma_8 = \sigma_8(H_0, \Omega_M, \Omega_\Lambda, \Omega_B, n \ldots)$, matching of the COBE [85] with the cluster abundance gives a significant constraint on cosmological parameters $\Omega_M = \Omega_M(H_0, \Omega_\Lambda)$ [79,86], which improves by adding small-angle CBR data [87–90]. The presence of the tensor mode makes the range of n more uncertain, but notwithstanding these uncertainties, $\Omega_M > 0.5$ is difficult to reconcile with the matching condition whereas too-small Ω_M ($\lesssim 0.15$) is not consistent with the cluster abundance. These constraints will rapidly improve with new CBR data.

20.3. The Cosmological Constant

20.3.1. ***Type Ia supernova Hubble diagram***: The luminosity distance receives a cosmology-dependent correction as z increases: Ω_M pulls down d_L and Ω_Λ pushes it up. In first order of z the correction enters in the combination of $q_0 = \Omega_M/2 - \Omega_\Lambda$, so this is historically referred to as a q_0 test, a measure of cosmic deceleration, although this single-parameter description is not adequate at the redshifts of the current samples. The discovery by two groups that distant supernovae are fainter than expected from the local sample, even fainter than expected for $q_0 = 0$, points to the reality of $\Lambda > 0$ [63,64]. The best fits are currently for $\Omega_\Lambda \approx 0.7, \Omega_M \approx 0.3$—a flat, Λ-dominated universe.

The challenge of this analysis is to differentiate among interesting cosmologies with small differences of brightness. The samples are on average about 0.25 mag fainter than in the $\Omega_M = 0.2$, $\Omega_\Lambda = 0$ model, a difference most economically explained by adopting a cosmology with $\Lambda > 0$. On the other hand, at $z = 0.4$ where many supernovae are observed, the difference is $\Delta m = 0.12$ mag between $(\Omega_M, \Omega_\Lambda) = (0.3, 0.7)$ and $(0, 0)$, and $\Delta m = 0.22$ from $(0, 0)$ to $(1.0, 0)$. Therefore, an accuracy of $\lesssim 0.05$ mag ($\lesssim 5\%$) must be attained including systematics to prove the presence of Λ without appeal to other constraints (on Ω_M, $\Omega_M + \Omega_\Lambda$, *etc.*). Each SN data point contains at best ± 0.2 mag (20%) statistical error; the question is whether the total error is mostly random and systematics are controlled to a level of $\lesssim 0.05$ mag. A particular difficulty arises from a procedure to match high z SNe with the template at $z \approx 0$, which involves an integration over SN spectra dominated by strong features as well as a careful calibration of the flux zero points at different color bands. Even for spectrophotometric standard stars, the synthetic magnitude usually contains errors of 0.02–0.05 mag, especially when the color band involves the Balmer or Paschen regions. Dust obscuration may also be amplified into an important potential source of error, since, for example, a 0.02 mag error in color results in a 0.06 mag error in A_V. Perlmutter *et al.* [64] estimate 0.02 mag and Riess *et al.* [63] (see also Ref. 91) estimate 0.03 mag for K correction plus zero point errors, and 0.025 and 0.06 for dust extinction errors, respectively.

20.3.2. ***Gravitational lensing frequencies for quasars***: The cosmological factor in the gravitational lensing optical depth is very sensitive to the cosmological constant, if $\Omega_\Lambda \gg \Omega_M$ [92,93]. On the other hand, it is nearly insensitive to the change of Λ when it is small ($\Omega_\Lambda \lesssim 0.6$, say); in that case the uncertainties in the normalization factor (galaxy number density and the mass distribution of galaxies) dominate. It is likely that $\Omega_\Lambda > 0.8$ is excluded. On the other hand, a more stringent limit or solid detection is liable to be elusive for a smaller Ω_Λ. Nearly a decade of continuous efforts have brought substantial improvement in reducing uncertainties in the normalization factor [94–96]. Nevertheless, the luminosity density of early type galaxies which dominate lensing is uncertain by about a factor of two. We should adopt a conservative limit at present $\Omega_\Lambda < 0.8$ which is insensitive to this concern.

20.3.3. ***Harmonics of CBR anisotropies***: The angular scale of the first acoustic peak is particularly sensitive to a combination of Ω_M and Ω_Λ. The position of the first acoustic peak as estimated numerically using CMBFAST [97] is

$$\ell_1 \approx 220 \left(\frac{1 - \Omega_\Lambda}{\Omega_M} \right)^{1/2} \quad , \tag{20.6}$$

valid to about 10% accuracy for the parameter range that concerns us. This means that the position of the acoustic peak is about $\ell \approx 220$ if $\Omega_M + \Omega_\Lambda = 1$, but it shifts to a high ℓ as $\Omega_M^{-1/2}$ if $\Omega_\Lambda = 0$. On the other hand, there is little power to determine Ω_M separately from Ω_Λ. The harmonics C_ℓ measured at small angles now reveal the acoustic peak [98], and its position favors a universe close to flat [87–89]. The most rescent result [99] indicates $0.88 \leq \Omega_M + \Omega_\Lambda \leq 1.12$, which means that a zero Λ universe is not tenable when combined with Ω_M from other arguments.

20.4. Conclusions

The status of Ω_M and Ω_Λ is summarized in Table 20.3. We have a reasonable convergence of the Ω_M parameter towards a low value $\Omega_M = 0.15$–0.4. The convergence of Ω_M is significantly better with the presence of a cosmological constant that makes the universe flat. Particularly encouraging is the agreement of Ω_M derived with the most reliable arguments. Even so, the current 'low Ω_M concordance' means values that still vary by more than a factor of two. The indication of $\Omega_\Lambda \neq 0$ from the SNeIa Hubble diagram is very interesting and important, but on its own the conclusion is susceptible to small systematic effects. On the other hand small-scale CBR anisotropy observations confirming a nearly flat universe, in combination with the sum of the other evidence considered here, strongly suggest the presence of Λ or other exotic (highly negative pressure) form of dark mass-energy.

In conclusion we present in Fig. 20.1 allowed ranges of H_0 and Ω_M (and Ω_Λ) for the case of (a) flat and (b) open universes. With the flat case we cut the lower limit of Ω_M at 0.2 due to a strong constraint from lensing. An ample amount of parameter space is allowed for a flat universe. A high value of $H_0 > 82$, which would be driven only by a short LMC distance, is excluded by self-consistency with the age of globular clusters, as

Table 20.3: Summary of Ω_M and Ω_Λ determinations.

Method	Ω_M	Ω_Λ
H_0 vs t_0	< 0.7	
luminosity density +M/L	0.1–0.4	
cluster baryon fraction	0.15–0.35	
SNeIa Hubble diagram	≤ 0.3	≈ 0.7
small-scale velocity field		
(summary)	0.2 ± 0.15	
(pairwise velocity)	0.15 ± 0.1	
(Local Group kinematics)	0.15 ± 0.15	
(Virgocentric flow)	0.2 ± 0.2	
large-scale velocity field	0.2−1	
cluster evolution		
(low Ω_M sol'n)	$0.2\,^{+0.3}_{-0.1}{}^*$	
(high Ω_M sol'n)	$\sim 1^*$	
COBE-cluster matching	0.35–0.45 (if $\Omega_\Lambda = 0$)*	
	0.20–0.40 (if $\Omega_\Lambda \neq 0$) *	
shape parameter Γ	0.2–0.4*	
CBR acoustic peak	$\approx (1 \pm 0.12) - \Omega_\Lambda{}^*$	$\approx (1 \pm 0.12) - \Omega_M$
gravitational lensing		< 0.8
Summary	0.15−0.45 (if open)	
	0.2−0.4 (if flat)	
		0.6−0.8

$*$CDM model used.

noted earlier. Therefore, we are led to the range $H_0 \approx 60$–82 from consistency. For an open universe the coeval-formation interpretation is compelling for globular clusters, or else no region is allowed; the allowed H_0 is limited to 60–70. No solution is available if LMC is at the shorter distance.

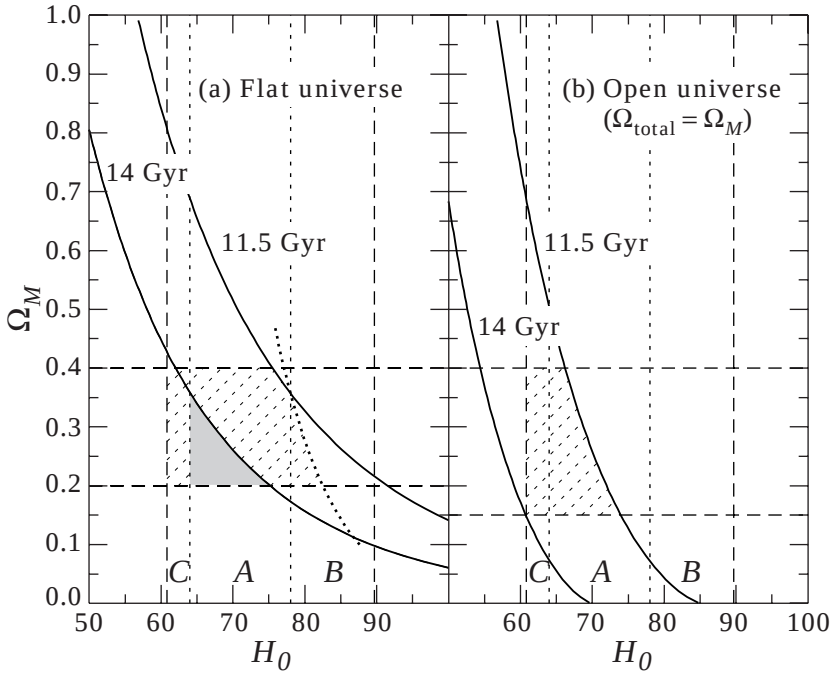

Figure 20.1: Consistent parameter ranges in the H_0–Ω_M plane for (a) a flat universe and (b) an open universe. A is the range of the Hubble constant when $(m - M)_{\rm LMC} = 18.5$. B is also allowed when the LMC distance is shorter by 0.3 mag, and C when longer by 0.1 mag. Note in panel (a) that most of the range of B is forbidden by the compatibility of age and H_0 that are simultaneously driven by the RR Lyr calibration (short dotted curve, see Sec. 20.1.6). Also note that the age range between ≈11.5 Gyr and ≈14 Gyr (light cross-hatched) is possible only with the interpretation that globular cluster formation is coeval (Sec. 20.1.5). The 'most natural' parameter region is dark gray.

References:

1. M. Fukugita, in *Structure Formation in the Universe*, Proc. of the NATO ASI, Cambridge, 1999 (to be published, 2000); `astro-ph/0005069`.
2. J.H. Jacoby *et al.*, Publ. Astron. Soc. Pac. **104**, 599 (1992).
3. W.L. Freedman *et al.*, Nature **371**, 757 (1994).
4. L. Ferrarese *et al.*, `astro-ph/9910501` (1999).
5. J.L. Tonry *et al.*, Astrophys. J. **475**, 399 (1997).
6. W.L. Freedman, B.F. Madore, and R.C. Kennicutt, in *The Extragalactic distance scale*, eds. M. Livio, M. Donahue, and N. Panagia (Cambridge University Press, Cambridge), p. 171 (1997).
7. J.L. Tonry *et al.*, Astrophys. J. **530**, 625 (2000).
8. S. Sakai *et al.*, Astrophys. J. **529**, 698 (2000).
9. D.D Kelson *et al.*, Astrophys. J. **529**, 768 (2000).
10. L. Ferrarese *et al.*, Astrophys. J. **529**, 745 (2000).
11. J.P. Blakeslee *et al.*, Astron. J. **527**, L73 (1999).
12. A.G. Riess, W.H. Press, and R.P. Kirshner, Astrophys. J. **438**, L17 (1995).
13. M. Hamuy *et al.*, Astrophys. J. **112**, 2398 (1996).
14. S. Jha *et al.*, Astrophys. J. Suppl. Ser. **125**, 73 (1999).
15. N.B. Suntzeff *et al.*, Astrophys. J. **117**, 1175 (1999).
16. B.K. Gibson *et al.*, Astrophys. J. **529**, 723 (2000).
17. A. Saha *et al.*, Astrophys. J. **522**, 802 (1999).
18. M.W. Feast and A.R. Walker, Ann. Rev. Astr. Astrophys. **25**, 345 (1987).
19. B.F. Madore and W.L. Freedman, Publ. Astron. Soc. Pac. **103**, 933 (1991).
20. F. van Leeuwen and C.S. Hansen-Ruiz, Mon. Not. of the R. Astron. Soc. **287**, 955 (1997).
21. J.-C. Mermilliod *et al.*, in *Hipparcos Venice '97*, ed. B. Battrick (ESA, Noordwijk, 1997), p. 643.
22. M.H. Pinsonneault *et al.*, Astrophys. J. **504**, 170 (1998).
23. V.K. Narayanan and A. Gould, Astrophys. J. **523**, 328 (1999).
24. M. Sekiguchi and M. Fukugita, Observatory **118**, 73 (1998).
25. M.W. Feast and R.M. Catchpole, Mon. Not. of the R. Astron. Soc. **286**, L1 (1997).
26. X. Luri, *et al.*, Astr. and Astrophys. **335**, L81 (1998).
27. B.F. Madore and W.L. Freedman, Astrophys. J. **492**, 110 (1998).
28. A. Udalski *et al.*, Acta Astron. **48**, 1 (1998).
29. K.Z. Stanek and P.M. Garnavich, Astrophys. J. **503**, L131 (1998).
30. E.F. Guinan *et al.*, Astrophys. J. **509**, L21 (1998).
31. A. Udalski *et al.*, Astrophys. J. **509**, L25 (1998).

32. R.G Gratton *et al.*, Astrophys. J. **491**, 749 (1997).
33. I.N. Reid, Astron. J. **114**, 161 (1997).
34. J. Fernley *et al.*, Astr. and Astrophys. **330**, 515 (1998).
35. A. Gould and P. Popowski, Astrophys. J. **508**, 844 (1998).
36. J.R. Herrnstein *et al.*, Nature **400**, 539 (1999).
37. E. Maoz *et al.*, Nature **401**, 351 (1999).
38. B.P. Schmidt, R.P. Kirshner, and R.G. Eastman, Astrophys. J. **395**, 366 (1992).
39. B.P. Schmidt *et al.*, Astrophys. J. **432**, 42 (1994).
40. S. Refsdal, Mon. Not. of the R. Astron. Soc. **128**, 307 (1964).
41. E.E Falco, M.V. Gorenstein, and I.I. Shapiro, Astrophys. J. **372**, 364 (1991).
42. T. Kundić *et al.*, Astrophys. J. **482**, 75 (1997).
43. G. Bernstein and P. Fischer, Astron. J. **118**, 14 (1999).
44. P.L. Schechter *et al.*, Astrophys. J. **475**, L85 (1997).
45. C.R. Keeton and C.S. Kochanek, Astrophys. J. **487**, 42 (1997).
46. F. Courbin *et al.*, Astr. and Astrophys. **324**, L1 (1997).
47. C.D. Impey *et al.*, Astrophys. J. **509**, 551 (1998).
48. A.D. Biggs *et al.*, Mon. Not. of the R. Astron. Soc. **304**, 349 (1999).
49. L.V.E. Koopmans and C.D. Fassnacht, Astrophys. J. **527**, 513 (1999).
50. M. Birkinshaw, J.P. Hughes, and K.A. Arnaud, Astrophys. J. **379**, 466 (1991).
51. S.T. Myers *et al.*, Astrophys. J. **485**, 1 (1997).
52. E.D. Reese *et al.*, Astrophys. J. **533**, 38 (2000).
53. A. Renzini, in *Observational Tests of Cosmological Inflation*, ed. T. Shanks *et al.*, (Kluwer, Dordrecht), p. 131 (1991).
54. D.A. VandenBerg, M. Bolte, and P.B. Stetson, Ann. Rev. Astr. Astrophys. **34**, 461 (1996).
55. B. Chaboyer, P. Demarque, and A. Sarajedini, Astrophys. J. **459**, 558 (1996).
56. A. Sandage, Astron. J. **106**, 703 (1993).
57. B. Chaboyer *et al.*, Astrophys. J. **494**, 96 (1998).
58. J.R. Mould *et al.*, Astrophys. J. **529**, 786 (2000).
59. N.A. Bahcall, L.M. Lubin, and V. Dorman, Astrophys. J. **447**, L81 (1995).
60. N. Kaiser *et al.*, `astro-ph/9809268` (1998).
61. M. Fukugita, C.J. Hogan, and P.J.E. Peebles, Astrophys. J. **503**, 518 (1998).
62. R.G. Carlberg, H.K.C. Yee, and E. Ellingson, Astrophys. J. **478**, 462 (1997).
63. A.G. Riess *et al.*, Astron. J. **116**, 1009 (1998).
64. S. Perlmutter *et al.*, Astrophys. J. **517**, 565 (1999).
65. W. Forman, and C. Jones, Ann. Rev. Astr. Astrophys. **20**, 547 (1982).

66. S.D.M. White *et al.*, Nature **366**, 429 (1993).
67. D.A. White and A.C. Fabian, Mon. Not. of the R. Astron. Soc. **273**, 72 (1995).
68. L. Grego *et al.*, presented at the AAS meeting (194.5807G) (1999).
69. P.J.E. Peebles, in *Formation of Structure in the Universe*, eds Dekel, A. and Ostriker, J. P. (Cambridge University Press, Cambridge), p. 435 (1999).
70. M. Davis and P.J.E. Peebles, Ann. Rev. Astr. Astrophys. **21**, 109 (1983).
71. M.A. Strauss and J.A. Willick, Phys. Reports **261**, 271 (1995).
72. A.J.S Hamilton, in *The Evolving Universe*, ed. D. Hamilton, (Kluwer, Dordrecht, 1998), p. 185.
73. A. Dekel *et al.*, Astrophys. J. **522**, 1 (1999).
74. G. Efstathiou, W.J. Sutherland, and S.J. Maddox, Nature **348**, 705 (1990).
75. J.A. Peacock and S.J. Dodds, Mon. Not. of the R. Astron. Soc. **267**, 1020 (1994).
76. V.R. Eke *et al.*, Mon. Not. of the R. Astron. Soc. **298**, 1145 (1998).
77. J.A. Peacock, Mon. Not. of the R. Astron. Soc. **284**, 885 (1997).
78. S.D.M. White, G. Efstathiou, and C.S. Frenk, Mon. Not. of the R. Astron. Soc. **262**, 1023 (1993).
79. V.R. Eke, S. Cole, and C.S. Frenk, Mon. Not. of the R. Astron. Soc. **282**, 263 (1996).
80. J. Oukbir and A. Blanchard, Astr. and Astrophys. **262**, L21 (1992).
81. R.G. Carlberg *et al.*, Astrophys. J. **479**, L19 (1997).
82. N.A. Bahcall and X. Fan, Astrophys. J. **504**, 1 (1998).
83. A. Blanchard and J.G. Bartlett, Astr. and Astrophys. **332**, L49 (1998).
84. D.E. Reichart, *et al.*, Astrophys. J. **518**, 521 (1999).
85. C.L. Bennett *et al.*, Astrophys. J. **464**, L1 (1996).
86. G. Efstathiou, J.R. Bond, and S.D.M White, Mon. Not. of the R. Astron. Soc. **258**, 1 (1992).
87. S. Hancock *et al.*, Mon. Not. of the R. Astron. Soc. **294**, L1 (1998).
88. C.H. Lineweaver, Astrophys. J. **505**, L69 (1998).
89. G. Efstathiou *et al.*, Mon. Not. of the R. Astron. Soc. **303**, 47 (1999).
90. M. Tegmark, Astrophys. J. **514**, L69 (1999).
91. B.P. Schmidt *et al.*, Astrophys. J. **507**, 46 (1998).
92. M. Fukugita, T. Futamase, and M. Kasai, Mon. Not. of the R. Astron. Soc. **256**, 25 (1990).
93. E.L. Turner, Astrophys. J. **365**, L43 (1990).
94. D. Maoz and H.-W. Rix, Astrophys. J. **416**, 425 (1993).
95. C.S. Kochanek, Astrophys. J. **466**, 638 (1996).
96. E.E. Falco, C.S. Kochanek, and J.A. Muñoz, Astrophys. J. **494**, 47 (1998).
97. U. Seljak and M. Zaldarriaga, Astrophys. J. **469**, 437 (1996).
98. P.F. Scott *et al.*, Astrophys. J. **461**, L1 (1996).
99. P. deBernardis *et al.*, Nature **404**, 955 (2000).